

Principles and in vivo Applications at High Field

Jérôme Voiron

Bruker BioSpin MRI GmbH, Ettlingen, Germany

Laurent Lamalle

INSERM, IFR n° 1 – Unité IRM 3 T, Centre Hospitalier Universitaire, Grenoble, France

Principles

Introduction

In magnetic resonance imaging (MRI) the signal to be sampled is equivalent to the spatial Fourier transform of the image to be reconstructed, and the sampling requirements common to all discrete Fourier methods apply. MRI techniques are typically described using \mathbf{k} -space formalism, where the spatial frequency vector \mathbf{k} (in m^{-1}) is given by the time integral of the magnetic field gradient vector \mathbf{g} (mT/m) experienced by the transverse magnetization during or before signal acquisition:

$$\mathbf{k}(t) = (\gamma / 2\pi) \int_{t_0}^t \mathbf{g}(\tau) d\tau \quad (1)$$

where $\mathbf{g} = \nabla |\mathbf{B}_0|$, \mathbf{B}_0 is the static polarizing magnetic field, and γ is the magnetogyric ratio (rad/T) of the nucleus under study (typically ^1H in H_2O). Note that the \mathbf{k} -space formalism assumes that both \mathbf{B}_0 and the pulsed magnetic field gradients $\mathbf{g}(t)$ are spatially homogeneous. The time origin t_0 corresponds to the time at which precessing transverse magnetization was created.

If we ignore spurious contributions to \mathbf{B}_0 and \mathbf{g} caused by residual field inhomogeneities (e.g., those associated with magnetic susceptibility variations across the sample) and transient eddy currents induced by gradient switching, then the field gradient waveform $\mathbf{g}(t)$ for spatial encoding simply follows the current waveforms applied to the gradient coils. As discussed below, the \mathbf{k} -space trajectory can have an arbitrary form, within the limits posed by the hardware employed. Key parameters are the maximal gradient strength G_{max} and the maximal gradient slew rate GSR_{max} (max. rate of variation).

The desired rectangular field of view for the acquired image (FOV, also denoted as ΔR_{max} in the following) and the spatial resolution $\delta \mathbf{r}$ of the image determine the characteristics of the Cartesian grid of points used to sample \mathbf{k} -space. The grid step size $\delta \mathbf{k}$ must be small enough (Nyquist criterion) to avoid

FOV aliasing artifacts (foldover) and the spatial frequency range covered (\mathbf{k} -space range ΔK_{max}) must be large enough to provide the desired resolution $\delta \mathbf{r}$ of the smallest structures or details of interest for the object under study. This leads to the following conditions, which are usually employed as equalities for setting up imaging experiments.

$$\text{FOV:} \quad \delta k_i \leq 1/\Delta R_{i,\text{max}} \quad (2)$$

$$\text{Resolution:} \quad \Delta K_{i,\text{max}} \geq 1/\delta r_i \quad (3)$$

where $i = x, y, z$ when a Cartesian coordinate system is employed. Alternatively, $i = r$ or p can be used to designate the so-called *read* and *phase-encoding* dimensions.

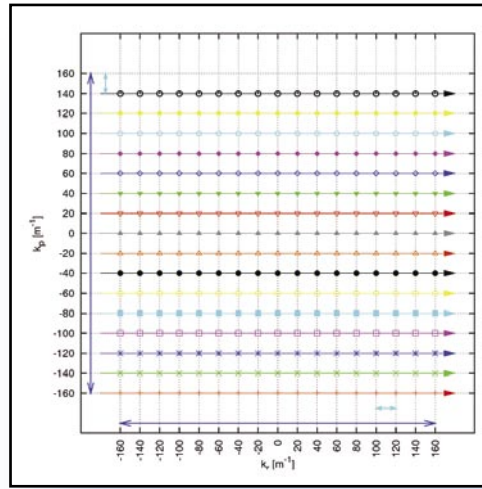


Fig. 1: Conventional 2D Cartesian \mathbf{k} -space sampling scheme. One k_x line is explored per rf excitation with repetition time TR and equidistantly sampled at the desired Cartesian grid points (individual line and point styles correspond to individual excitations). In this case an isotropic FOV has been chosen with $\Delta R_{\text{max}} = 50$ mm and an in-plane resolution $\delta r = 3.125$ mm in both dimensions. The long, dark-blue, double-headed arrows indicate ΔK_{max} (320 m^{-1}) along both the read and phase-encoding axes; the short, light-blue arrows designate the increment δk (20 m^{-1}).

Fig. 1 presents a schematic representation of a conventional two-dimensional \mathbf{k} -space sampling of an isotropic FOV. The raster range ΔK_{max} and the raster spacing δk for the read (k_x) and phase-encoding (k_y) directions are designated by long and short double-headed arrows. ΔR_{max} and δr can be similarly represented on the image pixel grid.

A Cartesian grid such as that in Fig. 1 can be sampled line by line using a read gradient G_r with constant amplitude applied during data acquisition for frequency encoding in the read dimension. Conventional MRI techniques require one rf excitation per line, with excitation being applied with the repetition time TR. The signal induced by the precessing M_{xy} magnetization is sampled by the digitizer (ADC) at constant time intervals (dwell time DW), resulting in a set of data points corresponding to equidistant \mathbf{k} -space samples along the read gradient axis (k_x). A second, orthogonal, spatial direction is explored using a corresponding phase-encoding gradient pulse G_p applied prior to acquisition before G_r is switched on. The amplitude of G_p is incremented in equal steps for each successive excitation to sample \mathbf{k} -space in the phase-encoding dimension (k_y). The linear variation of the integrals over G_r and G_p as \mathbf{k} -space is sampled along both the read and phase gradient axes is a highly desired property since constant intervals of frequency and phase evolution are

required for the straightforward use of the Fast Fourier Transform (FFT) algorithm for image reconstruction.

The total measurement time associated with the above scheme is given by the product $TR \cdot n_p$, where n_p is the number of phase-encoding steps, i.e., the number of k -lines acquired. The efficiency of data acquisition can be expressed as the ratio T_{acq}/TR , where T_{acq} is the actual time spent sampling the NMR signal during one TR period. Thus, to speed up the imaging process, a natural approach would be to look for a scheme that allows the acquisition of as many k -lines as possible per excitation (thus increasing T_{acq}/TR). For example, in the RARE spin-echo sequence a subset of n_p/n_{ex} k -lines in the read dimension can be sampled sequentially after one

Fig. 2: Schematic diagram of a 2D spiral MRI sequence using slice-selective excitation and FID or gradient-echo (GE) acquisition. The waveforms applied simultaneously to two orthogonal gradients (R and P) generate an outward spiral in k -space, as shown in Fig. 3.

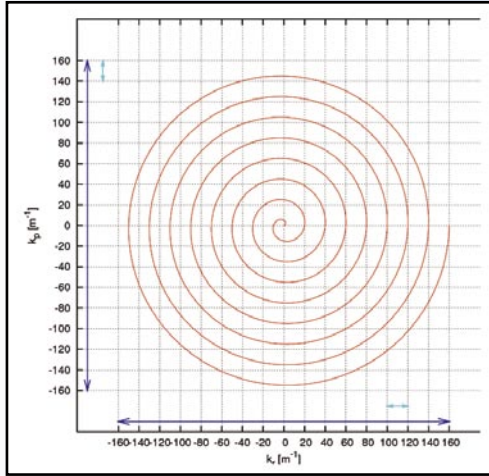
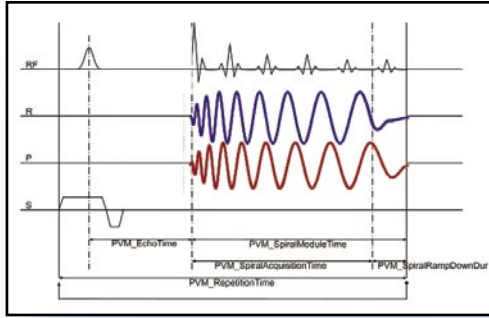


Fig. 3: Single-segment Archimedean outward spiral trajectory in k -space generated by the gradient waveforms of Fig. 2.

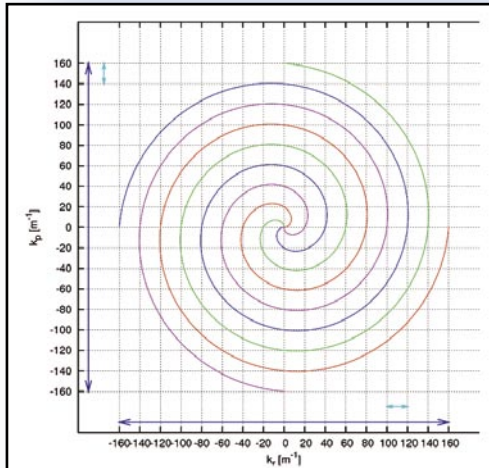


Fig. 4: Four-segment Archimedean spiral trajectories corresponding to $N_{\text{seg}} = 4$ (four excitations per image).

excitation by applying a 180° refocusing pulse between each acquisition period (echo). The parameter n_{ex} specifies the number of excitations used to cover all of k -space.

With the echo-planar imaging method (EPI) these additional 180° pulses can be avoided, and, in the ideal case, a complete set of k -lines can be acquired in an uninterrupted manner in a zigzag trajectory following a *single* excitation. Both RARE and EPI allow, in principle, the acquisition of a complete image after a single excitation (“single-segment” mode) or a small number of excitations (“multi-segment” or “interleaved” mode), resulting in a considerable improvement in time resolution with respect to conventional methods.

Like EPI, spiral imaging (**Fig. 2**) is a very fast MRI technique capable of sampling efficiently the entire k -space of interest in just one segment (**Fig. 3**) or in a few k -space segments (**Fig. 4**). Instead of using a zigzag trajectory to map out a Cartesian grid in k -space, spiral scanning typically uses an Archimedean spiral trajectory for the complex vector \mathbf{k}

$$\kappa(t) = \kappa_r(t) + i \kappa_p(t) \quad (4)$$

$$= \lambda \theta(t) \exp[i\theta(t)] \quad (5)$$

where the spiral radius $r = \lambda \theta(t)$ is defined to increase by one unit of the corresponding k -space Cartesian grid per revolution, i.e.

$$\lambda = \delta k / (2\pi) \quad (6)$$

as shown in **Fig. 3**. This scheme ensures that at least along the two Cartesian axes, the sampling criterion for correct FOV representation is satisfied.

With respect to spatial resolution, the number of spiral revolutions N_{turns} must be at least half the number of equidistant samples along the Cartesian axes. Thus, N_{turns} determines the range of the monotonic scalar function $\theta(t)$:

$$\theta_{\text{max}} = 2\pi N_{\text{turns}} \quad (7)$$

As discussed below, the characteristics of $\theta(t)$ can otherwise be chosen rather freely, within the constraints imposed by the gradient hardware (G_{max} and GSR_{max}). Since the spiral crosses both Cartesian axes the same number of times, one usually works with an isotropic (square) FOV with the same in-plane resolution in each dimension, and this situation will be assumed in the following. An anisotropic (rectangular) FOV with an appropriately scaled anisotropic spatial resolution is also possible but will not be considered further.

In the multi-segment mode with N_{seg} steps (equivalent to n_{ex}), the number of spiral rotations per segment is $N_{\text{turns}}/N_{\text{seg}}$, and the radial increment per revolution is increased by the factor N_{seg} , i.e.

$$\lambda = N_{\text{seg}} \delta k / (2\pi) \quad (8)$$

As illustrated in **Fig. 4** each spiral extends out to the limits of k -space, as defined by ΔK_{max} , but for each segment the spiral is rotated by $2\pi/N_{\text{seg}}$.

The next sections compare further features of EPI and spiral imaging, detailing somewhat the \mathbf{k} -space sampling considerations, the impact of gradient and digitizer hardware limitations, and the spiral imaging reconstruction strategy.

Considerations for \mathbf{k} -space sampling

In contrast to 2D EPI, which maps out a rectangular or square region of \mathbf{k} -space in Cartesian form, 2D spiral MRI explores an FOV which is essentially circular with diameter ΔK_{\max} and $N_{\text{turns}} = \Delta K_{\max} / (2\delta k)$. The area covered by the spiral is $\pi/4$ times that covered by a Cartesian grid of the same extent (ca. 78.5%) since the corners are not explored. If the spiral's maximum diameter is increased to $2^{1/2} \Delta K_{\max}$, the square Cartesian grid is then completely circumscribed by the circular border corresponding to the maximum spiral radius, but this is achieved at the expense of a factor $2^{1/2}$ or 41% more revolutions. Equal *areas* for the spiral and Cartesian grids are obtained when the spiral's outer diameter is $(4/\pi)^{1/2} \Delta K_{\max}$, which requires a ca. 13% increase in the number of revolutions N_{turns} compared with the original scheme. In practice, signal energy is generally heavily concentrated at the centre of \mathbf{k} -space so that the loss of some of the high spatial frequency components, corresponding to the corners of the Cartesian grid, is usually tolerable, and it is generally sufficient to use a spiral with outer diameter ΔK_{\max} . Note that by specifying a slightly higher spatial resolution (smaller δr) at a given FOV one can ensure \mathbf{k} -space coverage that is more rigorously equivalent to that of the standard Cartesian grid (see Eq. 3).

The Nyquist condition determines the minimal δk required to avoid aliasing in the FOV. With EPI, δk along the read axis is defined by the product $DW \cdot G_r$, and the chosen acquisition bandwidth $BW = 1/DW$ and the desired FOV are used to calculate the required G_r in a straightforward manner. For phase encoding a short gradient pulse G_p of area δk is applied between each read segment. If there were no time constraints due to finite gradient slew rates, the total data acquisition time would be just $DW(n_p \cdot n_r)$, where n_p and n_r are the number of data points or \mathbf{k} -space samples in the phase-encoding and read dimensions, respectively. The maximum gradient strength available on an imaging system will determine the shortest possible DW compatible with the required δk and image FOV. The higher the available bandwidth (digitization rate) and maximum gradient strength, the faster the image acquisition. Due to hardware or safety limits (e.g. electrostimulation phenomena), the gradient slew rate will always have a finite maximum value which determines the time required to switch the EPI read gradient from a positive to a negative value and vice versa. For a given gradient slew rate, the higher the G_r amplitude plateau, the longer it takes to switch polarity. Efficient data acquisition requires that the EPI signal be sampled not only on the G_r plateau but also during

the switching ramps between $\pm G_r$. In extreme cases the read gradient may have a sinusoidal form. Under such conditions the successive \mathbf{k} -space samples obtained will not be equidistant, and image reconstruction has to be adapted somewhat (EPI regridding). The ratio between the time spent on the ramps and the time spent on the plateau increases as DW is shortened to achieve the shortest acquisition time compatible with a given hardware.

In spiral MRI δk determines an upper bound for the radial increment between successive revolutions as well as for the angular or tangential increment between successive samples along the trajectory. In order to produce a $\mathbf{g}(t)$ integral (Eq. 1) that follows the spiral trajectory geometry imposed by the FOV

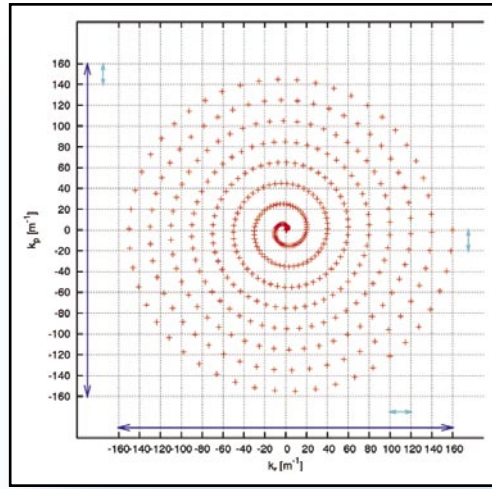


Fig. 5: Data sampling along a 2D spiral \mathbf{k} -space trajectory for the case of a linear $\theta(t)$, fulfilling the Nyquist criterion.

and spatial resolution constraints, the two orthogonal gradient current channels are modulated with similar oscillating but phase-shifted waveforms (see Fig. 2). This situation is quite different from that in the EPI experiment. The required gradient waveform can be derived from the time derivative of the desired \mathbf{k} -space vector.

$$\mathbf{g}(t) = (2\pi / \gamma) \frac{d}{dt} \mathbf{k}(t) \quad (9)$$

The minimum time required to traverse the complete trajectory will nevertheless depend also on the maximum gradient strength G_{\max} and the maximum slew rate GSR_{\max} . The instantaneous gradient slew rate $\mathbf{gsr}(t)$ associated with the spiral trajectory is given by:

$$\mathbf{gsr}(t) = \frac{d}{dt} \mathbf{g}(t) \quad (10)$$

Spiral trajectory optimization for high-speed imaging involves a search for the scalar function $\theta(t)$ that reaches θ_{\max} in the shortest possible time consistent with hardware constraints. If $\theta(t)$ were chosen to be linear in t , the calculations would be simple and a straightforward relation for the time proportionality constant would result. However, the gradient hardware would be underused. Glover [1] proposed an analytic

solution for $\theta(t)$ such that the gradient waveforms start with their highest slew rates (the peak amplitudes of the oscillations increase rapidly from zero) and are, therefore, in a regime limited by GSR_{\max} . As the trajectory progresses to the outer limits of the spiral, the peak amplitudes approach a plateau, and a second regime is entered where the limiting factor is G_{\max} .

Once a spiral trajectory time course has been defined, it is possible to specify the largest signal sampling time step compatible with the Nyquist condition. The tangential velocity along the spiral trajectory is highest at the periphery, where the maximum gradient amplitude is reached. Since DW is usually kept constant along the trajectory, the gradient characteristics as the last or outermost revolution of the spiral is performed will determine the minimal bandwidth (max. DW) required for resolution of the chosen tangential step δk , as illustrated in **Fig. 5** for the case of $\theta(t)$ linear in t . Higher digitizer sampling rates are possible, bringing some degree of tangential over-sampling which may be beneficial at the image reconstruction step.

Image Reconstruction

Regridding algorithm.

The Cartesian coordinates of the \mathbf{k} -space points sampled along spiral trajectories do not form a uniform grid (see Fig. 5); therefore, the FFT algorithm cannot be applied in the conventional manner for image reconstruction. A nonuniform discrete Fou-

rier transform (DFT) algorithm could be used but requires considerably more processing time. Thus, it is more efficient to interpolate the sampled data onto a Cartesian grid and then perform an FFT.

Interpolation or regridding of the discrete data points is performed by computing the convolution product of the sampled function with an analytic continuous function called the convolution kernel. The resulting convolution product is then a *continuous* function which can be re-sampled at regular grid coordinates. An appropriate choice for the convolution kernel will guarantee that the convolution product results in a good approximation of the function that was irregularly sampled. A sinus cardinal function has the disadvantage of not decreasing fast enough, thus resulting in a prohibitively long computation time. The standard convolution kernel chosen for this task is the Kaiser-Bessel function [2].

Once the \mathbf{k} -space data have been re-sampled on a Cartesian grid, the FFT algorithm can be applied for image reconstruction. However, it is necessary to take into account the effect of the convolution procedure performed in the Fourier domain; the transformed data must be divided by the Fourier transform of the convolution kernel. This latter operation has the undesirable effect of amplifying aliased noise at the edges of the FOV. To reduce this problem, the image is usually reconstructed with an extended FOV by using a \mathbf{k} -space re-sampling grid with step sizes that are half of those that would normally be required. This results in a doubling of data points in each dimension and a doubling of the FOV in each dimension. After FFT only the central part of the extended FOV will be retained, i.e., the originally planned number of data points and corresponding FOV.

The use of convolution products to compute interpolated data samples in \mathbf{k} -space is equivalent to estimating new data as weighted sums of the original noisy data. Fig. 5 shows that a spiral trajectory produces a higher density of sampled points in the central region of \mathbf{k} -space where the signal amplitudes and SNR are highest. As a side effect of data re-sampling onto a regular Cartesian grid, the original discrete signal is apodized so that the increased digitizer bandwidth used in spiral acquisition is benign in terms of SNR.

Trajectory measurement

Like EPI, spiral imaging is sensitive to several sources of artifacts. It is very important to ensure that the actual \mathbf{k} -space coordinates are accurately known. Several instrumental prob-

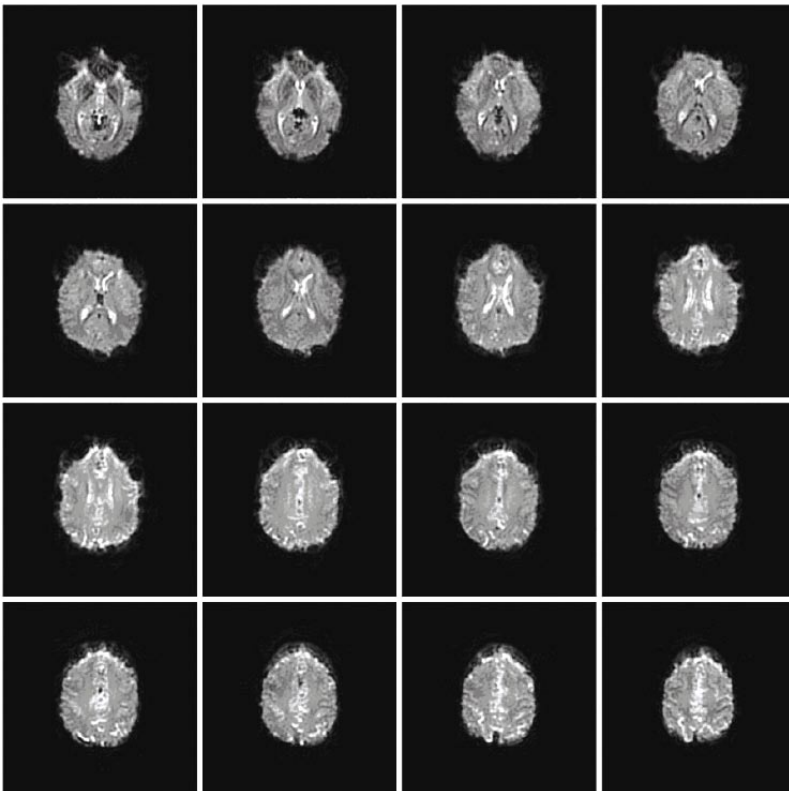


Fig. 6: Single-segment SPIRAL_OUT images obtained from the human brain during an fMRI protocol (self-paced finger tapping with the right hand) performed at 3T (MedSpec® S300). A set of 16 contiguous slices is shown, representing the central portion of the 35-slice data set obtained during one period of finger tapping (3-mm isotropic voxel resolution).

lems or limitations can cause the actual trajectory to differ from the planned or theoretically calculated one. Electronic delays in the gradient or rf hardware chains are a possible cause. Transient gradient terms associated with eddy currents induced by the pulsed gradients and residual B_0 inhomogeneities or susceptibility effects are additional factors which will influence $\mathbf{k}(t)$. Thus, it is advisable to calibrate the trajectory [3] using experimental conditions identical or very similar to those used for acquiring images.

Blurring artifacts

Like EPI, the spiral technique is very sensitive to B_0 inhomogeneity and to chemical shift effects. Robustness in this regard is increased through the use of the shortest possible acquisition times. B_0 inhomogeneities result in a blurring of the image, rather than the geometric distortion observed with EPI in the phase-encoding dimension. In contrast to EPI, spiral imaging features isotropic T_2^* and T_2 weightings, intrinsic apodization or \mathbf{k} -space weighting during acquisition, robustness to motion artifacts, the possibility of using a very short TE, and a T_{acq}/TR ratio which approaches the ideal value of 1.

High-Field Results

The following experimental results demonstrate the potential of spiral MRI, even at high B_0 field where field inhomogeneities and chemical shift effects combine to make the application of spiral imaging techniques more difficult.

All data were obtained with the SPIRAL method delivered with *ParaVision*® 4.0 and developed in a collaboration between Bruker BioSpin MRI and the Institut Fédératif de Recherche n°1, *RMN Biomédicale* (Grenoble, France).

fMRI of the human brain at 3 T

Experiments were performed to validate the SPIRAL method as a possible alternative to EPI for functional MRI of the human brain at 3 T. A time course of acquisitions was executed with the volunteer performing a simple self-paced finger-tapping motor task in an on/off manner. BOLD (Blood Oxygenation Level Dependent) T_2^* contrast was employed by sensitizing the MR signal to brain activation with a gradient-echo (GE) protocol with a TE of 30 ms, which seemed to be a good compromise for obtaining an adequate BOLD effect while preserving some robustness to B_0 inhomogeneity. The aim of the experiment was basic validation of the method and involved:

- checking that all post-processing steps used to analyze the functional time series were working as smoothly as in the case of EPI data acquisition;
- checking that activation maps could be obtained and that they made sense.

Methods

The study was performed at 3 T on a Bruker *MedSpec*® S300 whole-body scanner equipped with a B-GA63-HI gradient system (inner bore diam. = 63 cm, maximum gradient strength $G_{\text{max}} = 41$ mT/m, maximum slew rate $GSR_{\text{max}} = 141$ T/m/s) and a transmit/receive (TX/RX) quadrature rf coil designed specifically for human brain studies.

A healthy volunteer gave informed consent to participate in the experiment, which was performed according to the guidelines defined in a protocol agreed upon by an ethics committee. After orthogonal scout images were acquired, automatic localized shimming of B_0 homogeneity was done with FASTMAP, using all first- and second-order shim gradients. The FASTMAP voxel was adjusted to be the smallest cube which encompassed the whole brain. A sagittal localizer data set oriented on the inter-hemispheric plane was then acquired with a T_1 -weighted 3D FLASH sequence to locate the anterior and posterior commissures. The sagittal images were used to orient the spiral axial slices parallel to the bicommissural plane. Thirty-five interleaved, contiguous slices of 3-mm thickness were defined to cover most of the brain, in particular the motor areas.

The following acquisition parameters were used: slice excitation pulse = Hermite with 80° flip; in-plane FOV = 288×288 mm (to allow for possible off-center positioning of the subject); data matrix = 35 slices with 96×96 voxels and 3 mm isotropic resolution; acquisition bandwidth BW = 400 kHz; TR/TE = 2500/30 ms, single-segment gradient waveform = SPIRAL_OUT; maximum allowed slew rate = 90% of GSR_{max} ; FID acquisition (GE mode). The duration of the SPIRAL_OUT pulse sequence module was 36.35 ms. A fat-suppression preparation module was activated to avoid chemical-shift artifacts.

These parameters were equivalent to those used in analogous EPI protocols. Prior to acquisition of the time-course data, the \mathbf{k} -space trajectories were calibrated on the subject with

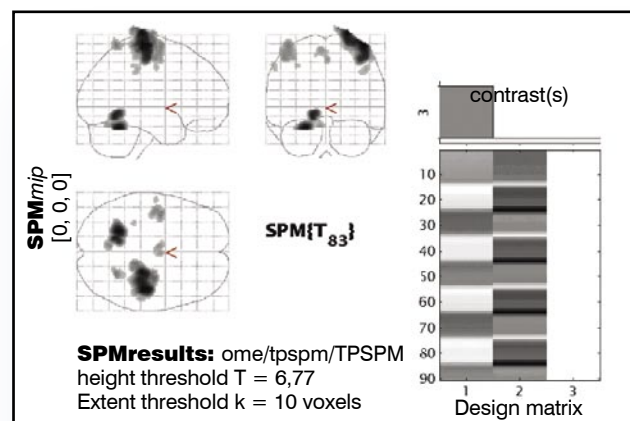


Fig. 7: Results of the fMRI finger tapping protocol, showing the statistical parametric mapping (SPM) design matrix (right), and brain activation maps (left).

the same parameter settings, except that the slice thickness for gradient calibration was set to 0.7 mm to reduce through-plane partial volume effects. The fMRI time course comprised 108 repetitions (NR) with a total scan time of less than 5 min. At the end of the protocol, high-resolution T_1 -weighted anatomic images were acquired with a 3D MP-RAGE sequence for activation localization.

The volunteer was instructed to perform a self-paced finger tapping task with the right hand according to a block paradigm. The *on* and *off* states of finger tapping were initiated by instructing the subject via a video display synchronized with the MRI acquisition. The “on” instruction was displayed in green letters, the “off” instruction in red letters. Twelve acquisitions were performed per block (block duration = 30 s), followed by a rest block. Four pairs of activation/rest cycles were repeated.

The data were converted to the Analyze image format, and the images from the functional time course were analyzed using the SPM2 software for statistical parametric mapping (Wellcome Department of Cognitive Neurology, London, UK). To correct for rigid body motion, all volumes were realigned on the last one obtained just prior to the anatomic scan. The anatomic scan data were normalized on the MNI (Montreal Neurologic Institute) template, and the normalization parameters obtained were applied to the functional data. Spatial smoothing with a $6 \times 6 \times 6$ mm Gaussian kernel was performed. A Student *t*-test was used to detect pixels with a mean “active” signal level that was significantly higher than the mean “rest” signal level.

Results and Discussion

Fig. 6 shows 16 central slices taken from the 35-slice data set acquired during finger tapping. **Fig. 7** shows the statistical parametric mapping (SPM) design matrix and three orthogonal views of the brain areas exhibiting statistically significant activation during finger tapping with the right

hand. As expected, the motor network was activated, i.e., in the contralateral primary sensory-motor area, in the ipsilateral cerebellum, in the supplementary motor area, and the ipsilateral primary sensory-motor area. In addition, the V4 visual area responsive to color was also activated, probably due to the contrast between the green and red characters used for the instructions display.

In Fig. 6 the expected signal losses associated with partial volume effects and local B_0 inhomogeneities were observed, particularly in the orbital frontal region. Overall image quality was quite comparable to that of EPI images routinely obtained with similar protocols.

All post-processing steps required for SPM could be applied to the spiral images exactly as with standard EPI data. The activation maps obtained were consistent with known behavior for the finger-tapping protocol. Thus, it should be worthwhile to investigate the possibilities of applying the SPIRAL method in more elaborate fMRI studies.

SPIRAL vs. EPI imaging of rat brain at 7 T

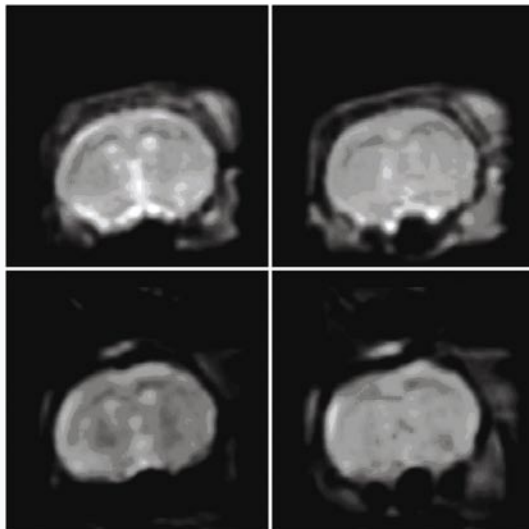
The SPIRAL method is an alternative to EPI for BOLD fMRI or for diffusion or perfusion imaging applications. Actually, the SPIRAL_OUT technique offers a clear advantage over EPI whenever a short TE and increased robustness to motion artifacts are of interest, as is typically the case with diffusion or spin-label perfusion experiments. Here we demonstrate the feasibility of spiral imaging on rat brain at high field and compare the short-TE performance of SPIRAL with that of EPI in the GE or SE acquisition modes.

Methods

The instrumentation used was a *PharmaScan*[®] 70/16 (7 T horizontal magnet with 16-cm bore diam.) equipped with the new B-GA9S gradient system ($G_{\max} = 366$ mT/m, $GSR_{\max} = 3424$ T/m/s) with high shim strength capabilities. A rat head resonator (birdcage, inner diam.: 38 mm) was used as TX/RX coil. Rats were anesthetized and maintained with isoflurane at 1 - 2.5%.

First- and second-order shim gradients were adjusted with FASTMAP over a cubic voxel (7.8 mm edge length) positioned in the front lobe of the rat brain, where all imaged slices were located. The transversal slice geometry and the isotropic in-plane parameters were identical for SPIRAL_OUT and EPI acquisitions in the GE or SE mode, and protocol timings were optimized in order to achieve as short a TE as possible while preserving reasonable values for all other parameters. Single-segment protocols were set up using a 30-mm FOV typically used for rat brain studies and employing 1-mm slices with 64×64 voxels (in-plane resolution: $469 \mu\text{m}$). To reduce the duration of the acquisition window and the sensitivity to B_0 inhomogeneity, four-segment GE and SE spiral protocols

Fig. 8: Single-segment GE spiral images (top row) and the corresponding EPI images (bottom row) of rat brain at 7 T. For each method two different transversal slices are shown (slice thickness: 1-mm, matrix: 64×64 , in-plane resolution: $469 \mu\text{m}$). The echo time TE and acquisition window duration were 1.1 ms and 12.1 ms for the SPIRAL protocol, 6.7 ms and 17.2 ms for EPI.



were also optimized and tested. In this case a 40-mm FOV was used with 96×96 voxels per slice for a small improvement in the in-plane resolution ($417 \mu\text{m}$). Slice excitation and refocusing (SE method) were achieved with 90° and 180° Hermite pulses with pulse lengths of 1.0 and 0.633 ms, respectively. Outer-volume suppression outside the FOV was performed using presaturation slices. Before SPIRAL or EPI acquisitions, trajectory calibration measurements were performed directly on the animal, using the parameter sets of the imaging sequences, with the exception of a smaller slice thickness (0.7 mm) to reduce through-plane partial volume effects.

Single-segment SPIRAL_OUT. Specific parameters were: FOV = 30 mm; 64×64 pixels per 1-mm slice; BW = 450 kHz; max. allowed slew rate = 90% of GSR_{max} ; spiral acquisition window duration = 12.1 ms per slice; $TE_{\text{min}} = 1.1/5.4$ ms for GE/SE mode; no fat suppression.

Single-segment EPI. FOV = 30 mm; 64×64 pixels per 1-mm slice; BW = 250 kHz due to hardware limits on the read gradient; max. allowed slew rate = 90% of GSR_{max} ; EPI acquisition window = 17.2 ms; $TE_{\text{min}} = 6.7/16.3$ ms for GE/SE mode; no fat suppression.

Four-segment SPIRAL_OUT. FOV = 40 mm; 96×96 pixels per 1-mm slice; BW = 450 kHz; max. allowed slew rate = 90% of GSR_{max} ; acquisition window = 4.9 ms per segment; $TE_{\text{min}} = 1.1/5.4$ ms for GE/SE; TR = 2000 ms. Fat suppression pulses were applied to reduce chemical shift artifacts.

Four-segment EPI. FOV = 40 mm; 96×96 pixels per 1-mm slice; BW = 345 kHz; max. allowed slew rate = 90% of GSR_{max} ; acquisition window = 7.9 ms per segment; $TE_{\text{min}} = 4.6/12.2$ ms for GE/SE.

Results and Discussion

For identical geometry specifications, the SPIRAL method, compared to EPI, allows the use of a shorter acquisition window and shorter TE, which provides improved image quality, as detailed below. We have not compared performance with identical echo times, but it is expected that the shorter acquisition window of SPIRAL should still be advantageous.

Fig. 8 compares GE images of 2 different slices obtained with either the single-segment SPIRAL (top row) or EPI (bottom row) protocols. The slightly higher signal intensity observed in SPIRAL vs. EPI images could be the result of the shorter TE in the spiral acquisition (1.1 ms vs. 6.7 ms) and less signal loss due to T_2^* relaxation. The shorter acquisition window or read duration for SPIRAL vs. EPI (12.1 ms vs. 17.2 ms) is associated with the shorter TE and can explain why spiral images apparently suffer less from B_0 inhomogeneity effects. However, the differences are difficult to quantify since the two methods respond differently to variations in B_0 : blurring in spiral images, geometric distortions in EPI. In any event,

the images shown suggest less distortion and somewhat better resolution of details in SPIRAL vs. EPI images (*corpus callosum* and definition of structural borders).

In the single-segment SE acquisition mode the difference in signal intensity for SPIRAL vs. EPI, as shown in **Fig. 9**, is

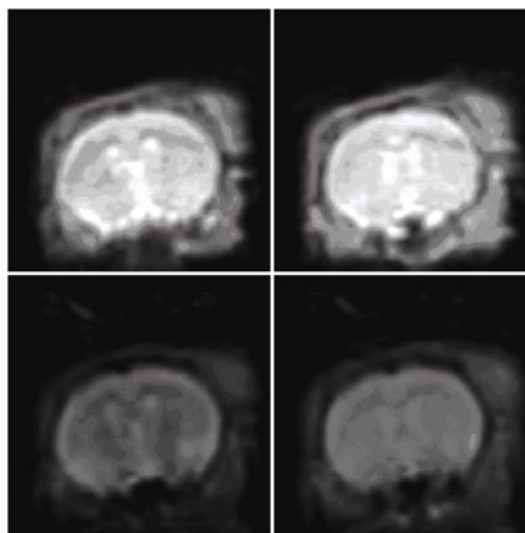


Fig. 9: Single-segment SE spiral (top row) and EPI (bottom row) imaging of rat brain at 7 T (same slice thickness and in-plane resolution as in Fig. 8). TE and acquisition window duration were 5.4 ms and 12.1 ms for SPIRAL, 16.3 ms and 17.2 ms for EPI.

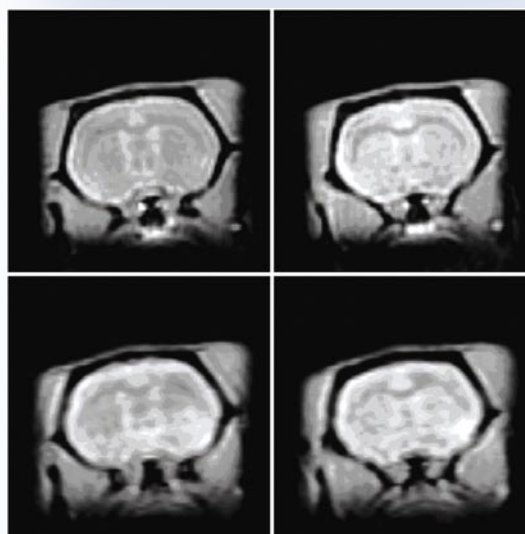


Fig. 10: Four-segment GE spiral (top row) and EPI (bottom row) imaging of rat brain at 7 T with fat suppression (slice thickness: 1-mm, matrix: 96×96 , in-plane resolution: $417 \mu\text{m}$). For the SPIRAL and EPI protocols TR/TE = 2000/1.1 ms and 2000/4.6 ms, respectively, and the acquisition window duration = 4.9 ms and 7.9 ms, respectively.

significantly larger than in the GE mode (Fig. 8). This can be explained by the much longer TE required by EPI (16.4 ms compared to 5.4 ms), which results in more pronounced signal attenuation via T_2 relaxation. As expected, for both techniques signal losses due to B_0 inhomogeneity effects are decreased in the SE images in comparison with the corresponding GE images, particularly for the lower parts of the brain.

The combined use of four-segment acquisition and fat suppression resulted in a dramatic improvement in GE image quality for both SPIRAL and EPI methods (**Fig. 10**), whereby the benefit of fat suppression is probably more important for spiral images where the shorter TE results in less

fat signal attenuation via relaxation. In general, the shorter acquisition window inherent with interleaving results in less geometric distortion or blurring, notably in the lower part of the brain. Since SPIRAL allows even shorter signal acquisition windows and TEs compared to EPI, the spiral images exhibit a higher quality with better resolution of structural details and borders (anatomical features such as the *corpus callosum*) and less image distortion.

Finally, the four-segment SE comparison with fat suppression (**Fig. 11**) also shows the significant advantage of SPIRAL over EPI in terms of signal intensity (less T_2 relaxation). Otherwise, through the combined use of SE acquisition and interleaving, both techniques provide comparable image quality.

Fast mouse brain imaging at 9.4 T

Here we demonstrate another animal brain study, this time with a mouse at 9.4 T using a Bruker CryoProbe™ surface coil. This cryo-cooled rf coil improves the SNR by about a factor of 2 and allows the imaging of much finer structural details.

Methods

A *BioSpec*® 94/20 system was equipped with the B-GA12S gradient coil ($G_{\max} = 482$ mT/m, $GSR_{\max} = 3798$ T/m/s) and a 20-mm CryoProbe™ as TX/RX surface coil. Mice were anesthetized and maintained with isoflurane at 1 - 2.5%.

First- and second-order shim gradients were adjusted with FASTMAP over a cubic voxel of 4-mm edge length positioned in the front lobe of the mouse brain, where all imaged slices were located. Eight-segment gradient-echo spiral protocols were set up for a 19-mm FOV, as typically used for mouse brain studies, employing 0.5-mm slices with 168×168 voxels (in-plane resolution: $113 \mu\text{m}$). Outer-volume suppression

outside the FOV was performed using a series of presaturation slices. To achieve standard T_2^* contrast, TE = 7 ms was used. For more flexibility the trajectories were calibrated directly on the animal, using the parameter sets of the imaging sequences, except that thinner slices (0.3 mm) were used to reduce through-plane partial volume effects.

Results and Discussion

High quality axial (**Fig. 12**) and coronal views (**Fig. 13**) of mouse brain were obtained in only 17.5 s. These images exhibit a high level of anatomical detail (*corpus callosum* and *cerebellum*) despite the very short acquisition time. Such structural details are normally difficult to record with fast imaging techniques such as EPI or spiral, and the image quality achieved was only possible through the use of the CryoProbe™ with its factor of 2 gain in SNR. Furthermore, the robustness of the spiral technique regarding motion is evident since no navigator signal was used to compensate for phase and amplitude variations between individual k -space segments.

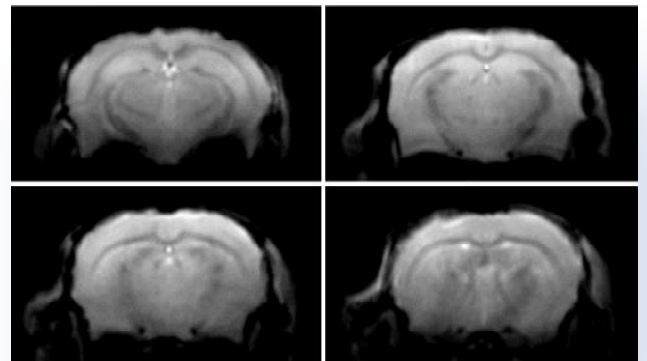


Fig. 12: Axial views of a mouse brain acquired in vivo at 9.4 T in a total measurement time of just 17.5 s. A 20-mm CryoProbe™ surface coil was used with an eight-segment GE spiral protocol (TR/TE = 2500/7 ms, with fat suppression, FOV = 19 mm, 0.5-mm slices with in-plane pixel resolution of $113 \mu\text{m}$).

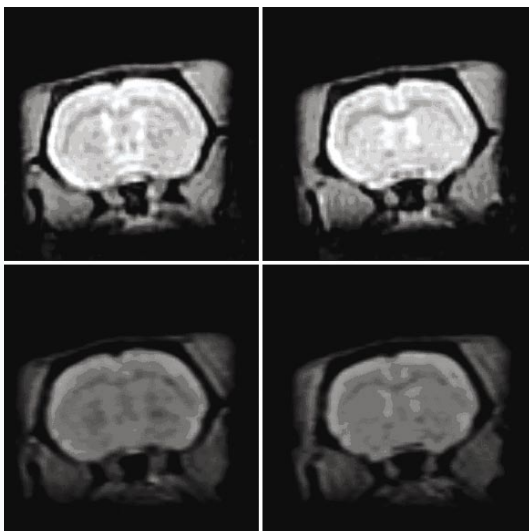


Fig. 11: Four-shot SE spiral (top row) and EPI (bottom row) images. TE/TR = 5.4/8000 ms and 12.2/8000 ms, respectively. The acquisition window duration was 4.9 ms and 7.9 ms for the spiral and EPI protocols, respectively. Fat suppression was activated.

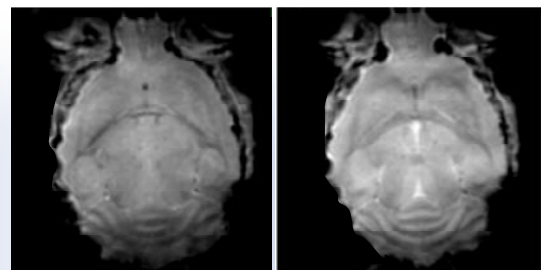


Fig. 13: Coronal slices of a mouse brain acquired as in Fig. 12.

Fast cardiac imaging of the rat at 7 T

We have seen above that spiral imaging techniques provide access to much shorter echo times compared to EPI methods. A further useful property of spiral techniques is their intrinsic

robustness with respect to motion artifacts. This advantage arises from the short acquisition window durations that can be achieved and the periodic moment nulling of both in-plane gradient waveforms used to create the k -space trajectory. Here we demonstrate the potential of multi-segment spiral GE acquisition for cardiac imaging.

Methods

The *PharmaScan*[®] 70/16 system with the B-GA9S gradient coil (see above) was used with a rat body resonator (birdcage with 60-mm inner diam.) as TX/RX coil. Rats were anesthetized and maintained with isoflurane at 1-2.5%.

Because shimming on the beating heart is difficult, the first- and second-order shims were optimized on the total active volume seen by the body resonator. The so-called short-axis view (a plane perpendicular to the interventricular septum and the long axis which passes through the apex of the heart) was localized with a T_2^* -weighted gradient-echo FLASH sequence (TR/TE = 8/2 ms).

For imaging of the cardiac cycle a single 1-mm transversal left-right (L-R) slice was positioned on the basis of the short-axis view. Slice excitation was performed with a 1-ms Hermite pulse and a flip angle of 20°. The spiral protocol (SPIRAL_OUT) was optimized to minimize TE (1 ms for our study). Parameters were set for an FOV of 50 mm and a reasonable in-plane resolution of 417 μm , a resolution considered mandatory for sufficient image quality. To minimize the acquisition window and the effects of strong local field inhomogeneities in the heart region, a bandwidth of 450 kHz (associated with an effective slew rate of 90% of GSR_{max}) and 20 k -space segments were chosen. Thus, an acquisition window of 1.6 ms per segment and TR of 12 ms were achieved. For a typical rat heart rate of 350 bpm, corresponding to 171 ms/cycle, such TR performance made it possible to record 12 frames of a cardiac movie over the cardiac cycle.

ECG and respiration signals of the rat were detected with a monitoring/gating device (SA Instruments) and used to synchronize (trigger) data acquisition at specific points in the cardiac/respiratory cycles. When the movie mode in the multi-segment SPIRAL method was activated, each segment (coding for the whole movie frame package) was appropriately synchronized with the rat ECG and respiratory signals. A navigator signal was used to compensate for phase and amplitude variations between individual k -space segments. The entire movie sequence was repeated for 10 averages, resulting in a total scan time of 29 s for a complete cardiac cycle.

Since cardiac motion prevented accurate *in vivo* trajectory calibration, the trajectories were measured on a completely homogeneous phantom (1 g/L CuSO_4 in water) using the parameter settings for cardiac imaging but with a slice thickness of 0.7 mm to reduce through-plane partial volume effects.

Results and Discussion

A cardiac movie comprising 12 image frames with 10 averages was acquired in 29 s, and the first frame is presented in **Fig. 14**. High contrast between blood volume and myocardium was achieved, and the resolution and SNR obtained are encouraging for further investigation of spiral techniques for fast cardiologic applications in the future. The use of post-processing software for analysis and quantification is also possible.

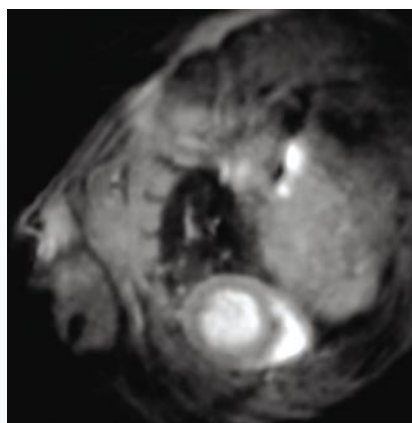


Fig. 14: In vivo cardiac imaging of the rat at 7 T using a 20-segment SPIRAL_OUT protocol. One image frame is shown from the 12-frame cardiac movie acquired in 29 s (10 averages) and covering the 171-ms cardiac cycle. Parameters were: axial oblique slice thickness: 1 mm, FOV = 50 mm, matrix: 120 × 120, in-plane pixel resolution: 417 μm , TR/TE = 12/1.0 ms.

Conclusions

The preliminary studies presented in this report provide validation of the SPIRAL_OUT method as a relevant and promising technique for functional MRI studies. Functional MRI studies can also take advantage of the SPIRAL_IN mode of acquisition, which enables an acquisition time per slice closer to the T_2^* of brain tissues and therefore a more efficient use of the available TR for acquiring more slices. Due to its ability to achieve shorter TEs, the SPIRAL method is likely to be a good alternative to EPI, especially for diffusion experiments. Finally, the SPIRAL technique can be optimized with acquisition windows that are shorter than those possible with EPI, resulting in fewer image artifacts. The implementation of additional SPIRAL features (navigator echo scheme) and applications (diffusion) is planned for the next *ParaVision*[®] release (> 4.0). Note that the modular software concept used to implement the SPIRAL acquisition modules means that future development of new SPIRAL techniques will not interfere with any customer-designed protocols based on the current version of the SPIRAL method.

References

- [1] Glover GH, Simple analytic spiral k-space algorithm, *Magn Reson Med* 42 (1999) 412-415.
- [2] Jackson JI, Meyer CH, Nishimura DG, Macovski A. Selection of a convolution function for Fourier inversion using gridding. *IEEE Trans Med Imaging* 10 (1991) 473-478.
- [3] Zhang Y, Hetherington HP, Stokely EM, Mason GF, Twieg DB. A novel k-space trajectory measurement technique. *Magn Reson Med* 39 (1998) 999-1004.